JOURNAL OF APPLIED ELECTROCHEMISTRY **27** (1997) 635–642

Structural changes induced by chemical reduction of various MnO_2 species

F. JEAN, C. CACHET, L. T. YU*

Laboratoire d'Electrochimie Catalyse et Synthèse Organique, Unité mixte Centre National de la Recherche Scientifique-Université de Paris-Val-de Marne, 2-8 rue H. Dunant 94320 Thiais, France

A. LECERF

Laboratoire de Chimie des Matériaux Inorganiques et de Cristallographie, 20 Avenue des Buttes de Coesmes INSA de Rennes, 35043 Rennes Cedex, France

A. QUIVY

Centre d'Etudes de Chimie Métallurgique, 15 rue G. Urbain 94400 Vitry-sur-Seine, France

Received 24 January 1996; revised 21 October 1996

Several kinds of MnO_2 were progressively reduced by cinnamic alcohol (CA) and aqueous hydrazine solutions (AHS) to compare changes in their structure. With α-MnO_2 stabilized by NH_4^+, the maximum homogeneous degree of H-insertion (MHID) is only 0.62 H per Mn, which involves the filling of each NH_4^+-free tunnel by four protons. This MHID value is consistent with the discharge capacity during the electrochemical reduction in 1 M KOH solution and in nonaqueous media (~0.65 and ~0.63 faradays per Mn, respectively). This result shows that Li^+ and H^+ ions occupy the same sites. The lowest degrees of oxidation are obtained when AHS are used, resulting in progressive appearance of a spinel structure which replaces the original lattice. For degrees of reduction x lower than $MnO_{1.33}$, pyrochroite exists in a poorly crystallized form since it is not observed in the XRD patterns. The XRD patterns of γ-MnO_2 reduced to $MnO_{1.12}$ usually show the spinel structure while the patterns of the Bi-doped MnO_2 reduced to $MnO_{1.14}$ exhibit peaks corresponding to pyrochroite and bismite (Bi_2O_3). Thus, the presence of Bi^{3+} hinders the formation of the nonelectroactive compound Mn_3O_4 or γ-Mn_2O_3, but the mechanism to explain this cannot be determined by XRD data alone.

1. Introduction

Manganese dioxide is the positive active material widely used in Leclanché and alkaline batteries, and more recently in lithium batteries. Since the early eighties, MnO_2 has been the object of investigation as a rechargeable positive electrode in alkaline media [1–12] or in the nonaqueous solvents used in lithium ion batteries [13, 14]. For these fields of application, the study of the structure versus the degree of reduction is of great interest because it provides information on the basic mechanism of its performance as a battery material. Up to now, most studies related to the evolution of the lattice during reduction have concerned γ-MnO_2 [15–24] which is widely used in the primary battery. They have shown that the first step is the insertion of protons into the lattice which is not destroyed but only expanded. The expansion is first isotropic then anisotropic [16, 20, 24]. During the second step, when the degree of H-insertion is higher than 1 H per Mn-atom (H/Mn), the spinel structure progressively appears. In most cases it is ascribed to Mn_3O_4 (hausmanite) or sometimes to γ-Mn_2O_3 since these two compounds both have the spinel structure.

Similar studies have been carried out on α-MnO_2 electrochemically reduced in various aqueous media [15–17, 25, 26] or chemically reduced [27]. As for γ-MnO_2, the first step in the reduction of α-MnO_2 is the insertion of protons into the lattice. Vosburgh [16] found that the resulting expansion of the α variety was smaller than in the case of the γ one. More recently, Gehain *et al.* [27] observed this phenomenon. They also notice a change of symmetry, which is attributed to an increase of the mean Mn ionic radius. Beyond 0.7 H/Mn, they note a collapse of the cryptomelane structure and the appearance of pyrochroite ($Mn(OH)_2$) and a spinel structure. According to Bode [19], the end of the homogeneous reduction occurs at 0.26 H/Mn and Mn_3O_4 is the resultant product. These values are low compared with the value found by Gehain *et al.* [27]. δ-MnO_2 has also been studied recently by Donne *et al.* [28]. The results show that this form has a behaviour similar to that of γ-MnO_2. The first step in the reduction is also a homogeneous process, but the spinel structure appears at about 0.5 H/Mn instead of 1 H/Mn for γ-MnO_2.

* To whom correspondence should be addressed.

The rechargeability depends on numerous factors such as the electrode characteristics, for example, the type and the quantity of carbons present [3, 8]. In practice, the discharge capacity is never higher than 0.50–0.6 faraday per Mn (F/Mn) instead of the expected 2 F/Mn due to the reduction of Mn(IV) to Mn(II). With a nonoptimized γ-MnO_2-electrode the cycle life number is only about 50 when the discharge is 0.35 F/Mn, and reaches 100 for an optimized electrode device. With a discharge depth of about 0.5 F/Mn, the cycle life number falls to 10 and 50, respectively [4–8]. With electrodeposited MnO_2 produced at very low temperatures, the cycle life number also reaches 100 and more for a discharge of about 0.53 F/Mn [12]. Nevertheless, the main limiting cause of the performance is the formation of the spinel structure, usually attributed to Mn_3O_4 [20–22] which is poorly electroactive. Thus, it is important to know the conditions in which spinel structure appears during discharge. Since the late 1980s, some authors [9–11, 13, 29, 30] have carried out discharges exceeding 1 F/Mn for chemically and physically modified manganese dioxides. These compounds are layer-like manganese dioxide containing foreign cations. The best results are obtained with the cations Bi^{3+} and Pb^{2+} [9, 10].

Therefore, in this paper we describe the structural changes as a function of the degree of the H-insertion in αMnO_2 stabilized by NH_4^+, a layer-like MnO_2 doped by Bi(III), and for the purposes of comparison, a common γ-MnO_2. As a consequence we, in particular, discuss the lodging sites for H-atoms and Li-atoms in α-MnO_2 structure.

2. Experimental details

The X-ray diffraction patterns were obtained using a Philips powder diffractometer equipped with a curved graphite monochromator in the diffracted beam (CoK_α radiation). To facilitate the reading, the various manganese dioxide samples will be subsequently labelled α-MnO_x for NH_4^+–α-MnO_2, γ-MnO_x for γ-MnO_2, Bi–MnO_x for Bi-doped δ-MnO_2. Although it is not strictly correct, but for the sake of convenience, x will be subsequently used for the degree of oxidation of the sample MnO_x.

The thiosulfate and Eriochrome-black-EDTA method gives the value of x [31]. Over the homogeneous reduction range, we use either x or y, the degree of H-insertion in MnO_2H_y (according to Tye's paper [23]). Thus, the relationship between x and y is

$$x = 2 - y/2 \quad (1)$$

γ-MnO_2 has been studied by many authors, among them Gabano *et al.* [18] and Tye *et al.* carried out a thorough study of the evolution of the homogeneous structure [23]. We studied a commercial product, purchased from Tekkosha (G.H. type). It contains 59.5 wt % (w/o) Mn (or 94.1 w/o pure MnO_2). Thermogravimetric measurements indicate 3.65 w/o water is removed at temperatures above 150 °C [32]. According to Ruetschi's model, this structural water corresponds to about 7% Mn^{4+} vacancies [33]. In addition, there is 2–3 w/o adsorbed water.

The δ-MnO_2–Bi samples contain 0.1 Bi(III) ion and about 1 H_2O molecule per Mn-atom. It is produced by a reduction reaction due to the protons in solution of 0.4 M $KMnO_4$ in 0.5 M nitric acid, at room temperature [34], in the presence of 0.04 M $Bi(NO_3)_3$.

α-MnO_2 was obtained by the oxidation of Mn(II) with solid $(NH_4)_2S_2O_8$ [35, 36]. All the α-MnO_2 samples were reduced for 5 h, but at different temperatures (see Table 1, column B), by cinnamic alcohol in xylene and stored at room temperature for two months. This long storage, described by Tye *et al.* [23], produces a uniform proton distribution throughout the lattice of the dioxide. We obtained

Table 1. Conditons of the chemical reduction of NH_4^+-doped α-MnO_2 by cinnamic alcohol and resulting chemical characteristics

A	*B*	*C*	*D*	*E*	*F*	*G*	*H*
Sample ref.	*Reduction temp* / °C	*x in MnO_x*	N / wt %	*Mn* / wt %	*S* / wt %	*C* (wt %)	*NH_4^+/Mn* (molar ratio)
CA1	not reduced	1.93	1.80 *0.128*	58.20 *1.06*	1.3 *0.041*	< 0.2	0.121
CA2	21	1.83	1.78 *0.127*	58.47 *1.06*	1.4 *0.043*	< 0.2	0.119
CA3	45	1.81	1.79 *0.128*	58.47 *1.06*		< 0.2	0.120
CA4	60	1.76	1.82 *0.130*	58.89 *1.07*		< 0.2	0.121
CA5	60	1.73	1.58 *0.113*	57.50 *1.05*		< 0.2	0.108
CA6	75	1.68	1.56 *0.111*	57.25 *1.04*		< 0.2	0.106
CA7	90	1.67	1.55 *0.111*	57.89 *1.05*		< 0.2	0.105

Sample CAI is not reduced.
In the columns D, E and F, the values written in italics refer to the mole of N, Mn and S per 100 g of sample, respectively. Those written in normal style correspond to contents expressed in g per 100 g of sample. Column H concerns the molor ratio NH_4^+/Mn.

different samples with x values in MnO_x ranging from $x = 1.88$ to $x = 1.67$. Even with a large excess of cinnamic alcohol, we never achieved lower degrees of oxidation. The N atom and Mn atom contents are listed in Table 1, columns D and E, respectively.

The molar ratio NH_4^+ / Mn of the initial sample is 0.121. The positive charge, due to NH_4^+, is compensated by a lowering of the average degree of oxidation of the Mn-atoms which is determined by

$$2z = 0.121 \tag{2}$$

Titration gave $2z = 0.140$. The difference between these two values are within the measurement accuracy. Therefore, there is no significant amount of Mn^{3+} in NH_4–MnO_2. Thus, the Relationship 1 must be modified:

$$x = 2 - z - (y/2) \qquad \text{for } z = 0.07 \tag{3}$$

To obtain samples with $x < 1.5$, hydrazine was used in aqueous solution. The temperature was maintained at 40 °C for 2 h and the degree of reduction was controlled through the excess of hydrazine (Table 2).

From the analysis of Tables 1 and 2 we note the following:

(i) Supposing that Mn, N, and S atoms are present in the form of MnO_2, NH_4^+, and SO_4, respectively, the overall elemental analysis balance, *Bal*, of the nonreduced sample (sample CA1) is

$$Bal = 87 \times 1.06 + 18 \times 0.128 + 96 \times 0.041 = 98.5 \text{ g}/100\text{g} \tag{4}$$

where 87, 18, and 96 are the molar weights of MnO_2, NH_4^+, and SO_4^{2-}, respectively. Such a balance is very close to 100%. The difference between 100 and *Bal* (~1.5%) is within the experimental error. Therefore, the quantity of Mn^{4+}-vacancies can be considered as negligible.

(ii) The ratio NH_4^+ (mol)/Mn (mol) does not vary when x is higher than 1.75.

(iii) As x decreases to 1.67, the decrease in the Mn content does not exceed 1%, which can be explained through the homogeneous insertion of H. The overall reaction according to Tye [23] is

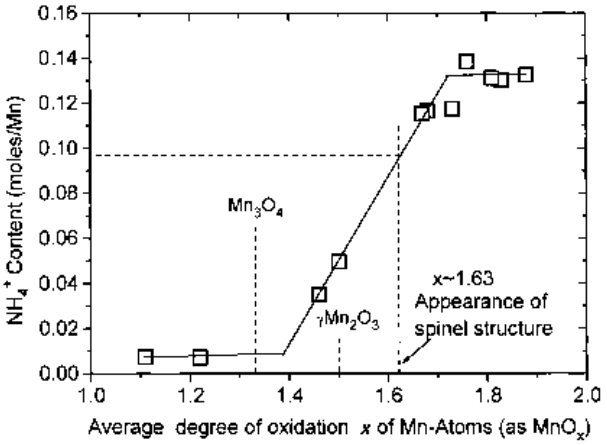

Fig. 1. Variation of the NH_4^+ content (expressed as mole/Mn) against the average degree of oxidation x (MnO_x).

$$MnO_2 + yH^+ + ye^- \rightarrow MnO_2H_y \tag{I}$$

where $y < 0.66$. The addition of y grams to 87 g, the molarweight of MnO_2, leads to a variation of the Mn content less than 1% . From $MnO_{1.67}$ to $Mn_{1.50}$, the Mn content increases by about 6%. Such an increase can be explained by the formation of a spinel structure γ-Mn_2O_3 or Mn_3O_4 from MnOOH, which involves a loss of water molecules, and thereby an increase of the Mn content in the resulting product by about 11.4 and 13.2%, respectively. For x less than 1.50, the Mn content varies within 1%, which is less than the experimental error. Such small variations can be ascribed to the formation of pyrochroite $Mn(OH)_2$ from MnOOH, which involve the insertion of 1 H-atom: for example, 1 g per 87 g of MnO_2. This is also within the experimental error.

Figure 1 shows the variation of the molar ratio NH_4^+/Mn against x. Due to the scatter in the data, we consider there is no significant variation when x is >1.67, When x is varying from ~1.67 to ~1.4, we observe a strong decrease in the molar ratio.

Table 2. Conditons of the chemical reduction of NH_4^+–α-MnO_2 by hydrazine and resulting chemical characteristics

A	*B*	*C*	*D*	*E*	*F*	*G*	*H*
Sample ref.	*Solution concentration*	*Reduction temp* / °C	*x in MnO_x*	*N* / wt %	*Mn* / wt %	*S* / wt %	*NH_4^+ / Mn* (molar ratio)
H1	1.75%	20	1.63				
H2	1.75%	40	1.56				
H3	1.75%	50	1.53				
H4	2.00%	40	1.50	0.68 *0.049*	61.57 *1.12*	1.2 *0.038*	0.044
H5	2.10%	40	1.46	0.5 *0.035*	60.28 *1.11*		0.032
H6	2.75%	40	1.22	0.1-0.2 *0.007*	61.55 *1.12*		0.006
H7	3.5%	40	1.11	0.1 *0.007*			

In the columns E, F and G, the values written in italics refer to the mole of N, Mn and S per 100 g of sample, respectively.

3. X-ray diffraction patterns

3.1. α-MnO_2

All the patterns show wide peaks. Thus, a quantitative treatment cannot be completed from the intensities. Figures 2 and 3 show the X-ray patterns of samples progressively reduced by cinnamic alcohol and hydrazine, respectively. Samples α-$MnO_{1.93}$ to α-$MnO_{1.67}$ (Fig. 2) and sample α-$MnO_{1.63}$ (Fig. 3) exhibit four major peaks of the cryptomelane structure, at $2\theta \simeq 14.6°$, $20.8°$ $33.4°$ and $43.5°$ indexed (1 1 0), (2 0 0), (3 1 0) and (2 1 1), respectively

Figures 4 to 7 show the variation of the d spacing of these peaks against the H-insertion level y. For the peaks (1 1 0) and (2 0 0), the d spacing increases until ~0.3 ± 0.015 H/Mn and remains constant. For the peak (3 1 0), an increase is observed over all the range (0–0.6 H/Mn), but a change in slope occurs at about 0.3 ± 0.015 H/Mn. Finally, for peak (2 1 1), the d spacing follows the same evolution as the peaks (1 1 0) and (2 0 0), but the change in slope occurs at 0.50 H/Mn only. These variations are similar to those observed by Gehain *et al.* [27] on cryptomelane containing K^+, but the changes in slope occur at $y \simeq 0.4$. Therefore, we agree with the conclusions of these authors, who assume the reduction process is due to the insertion of protons into the solid phase, and the various transitions are due to a variation of the crystal symmetry.

For samples α-$MnO_{1.56}$ to α-$MnO_{1.46}$, (Fig. 3) the new peaks at $2\theta \simeq 37.6°$ and $42.1°$ reveal the presence of a spinel structure. Some peaks (lettered P) can be attributed to the pyrochroite structure, but the peak at $2\theta \sim 18$ is not observed. These peaks disappear for the more reduced samples. The peaks due to the spinel structure progressively increase and those of cryptomelane progressively decrease. With α-$MnO_{1.46}$, the hollandite structure is still visible. With samples α-$MnO_{1.22}$ and α-$MnO_{1.11}$, only spinel peaks are observed, but their degrees of oxidation are lower than $MnO_{1.33}$, the degree of oxidation of hausmanite. Furthermore, the end-product is α-$MnO_{1.11}$ instead of the expected α-$MnO_{1.00}$ in spite of a large excess of hydrazine. Thus, such a low degree of oxidation involves the existence of pyrochroite in addition to hausmanite or γ-Mn_2O_3, but the XRD pattern does not show the corresponding peaks. Therefore, the pyrochroite obtained in these conditions has not a long-range crystallized structure.

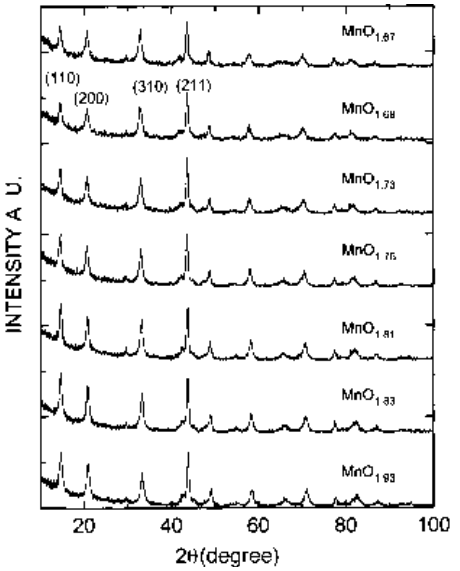

Fig. 2. Evolution of the XRD patterns of NH_4^+-doped α-MnO_2 samples (x = 1.88 to 1.67) reduced by cinnamic alcohol.

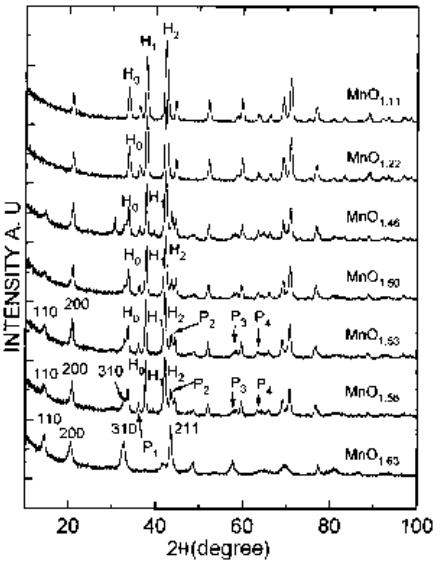

Fig. 3 Evolution of the XRD patterns of NH_4^+-doped α-MnO_2 samples reduced by hydrazine. H_0, H_1, H_2, correspond to the spinel structure P_1, P_2, P_3 and P_4, are attributed to pyrochroite. The ciphers concern the cryptomelane structure.

3.2. δ-MnO_2 *and* γ-MnO_2

The XRD patterns of Bi-doped δ-MnO_2 progressively reduced down to Bi–$MnO_{1.50}$ have the same aspect (Fig. 8(a)) as that of the pattern recorded by Donne *et al.* [28] on a synthetic δ-MnO_2 produced as a byproduct of saccharin manufacture. All these patterns show very broad peaks which correspond to a poorly crystallized compound having a layer-like structure (peak at $2\theta \simeq 18.20°$).

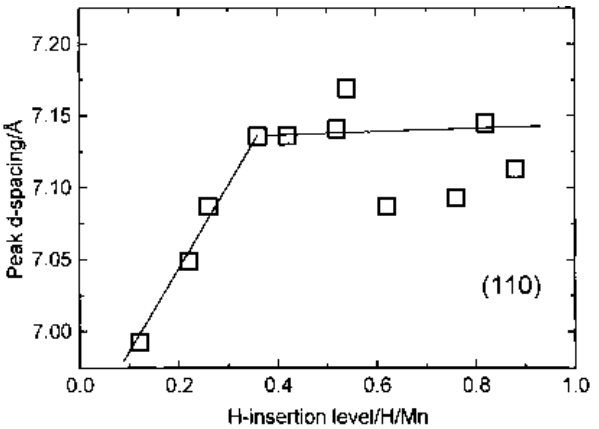

Fig. 4. Evolution of the peak d spacing against the H-insertion level for peak (1 1 0).

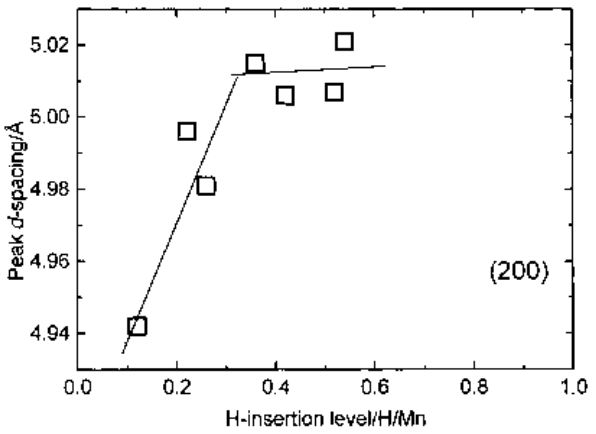

Fig. 5. Evolution of the peak *d* spacing against the H-insertion level for peak (2 0 0).

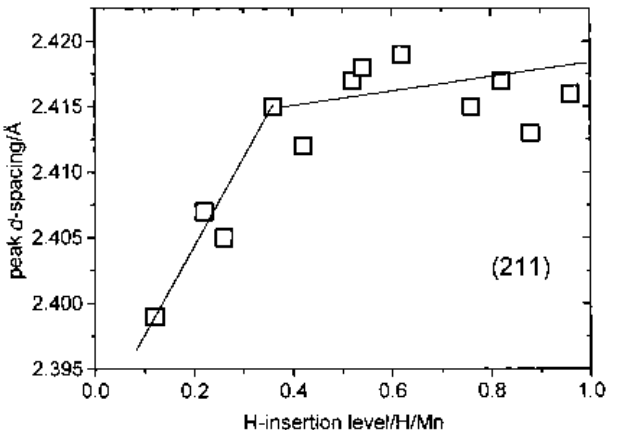

Fig. 7. Evolution of the peak *d* spacing against the H-insertion level for peak (2 1 1).

Figure 9(a) shows the XRD pattern of γ-MnO_3 in the initial oxidation state γ-$MnO_{1.96}$ and Fig 9(c) concerns the γ-$MnO_{1.12}$ sample. We again found the general shape of the patterns of electrodeposited manganese dioxide published elsewhere by various authors [37]. The latter is quasi-identical to the pattern of hausmanite (Fig. 9(b)). In spite of the low average degree of oxidation of $MnO_{1.12}$, the peaks of the spinel structure are still observed and the peaks due to pyrochroite are missing. These results show, on the one hand the difficulty in reducing the spinel structure, on the other hand pyrochroite is ill-crystallized over a long spatial range.

With the Bi–$MnO_{1.04}$ sample, the XRD pattern (Fig. 8(b)) is dominated by the peaks of Bi_2O_3 (bixmite). According to the results of Donne *et al.* [28], the peaks of the spinel structure should be observed. Thus, the presence of Bi prevents the formation of the spinel structure. Additionally, peaks involving Bi-atoms are not observed in the patterns of the Bi–$MnO_{1.88}$ and Bi–$MnO_{1.50}$ samples. Therefore, during the reduction of Mn(III) into Mn(II), phase separation takes place.

Furthermore, with Bi–$MnO_{1.04}$ samples, a wide peak at $2\theta \simeq 23°$ is observed. This indicates the existence of a layer-like structure, and thereby a pyrochroite-like compound. These results show that Mn(II) does not form a long range crystallized structure. The MnO_2 matrix keeps its initial ill-crystallized structure when the oxidation state varies from Bi–$MnO_{1.94}$ to Bi–$MnO_{1.04}$.

Finally, Bi-doped MnO_2 samples are characterized by the absence of the spinel structure when they are reduced to oxygen content less than $MnO_{1.5}$. This contrasts with the other forms of MnO_2 and their analogues which show the presence of the aforesaid spinel structure.

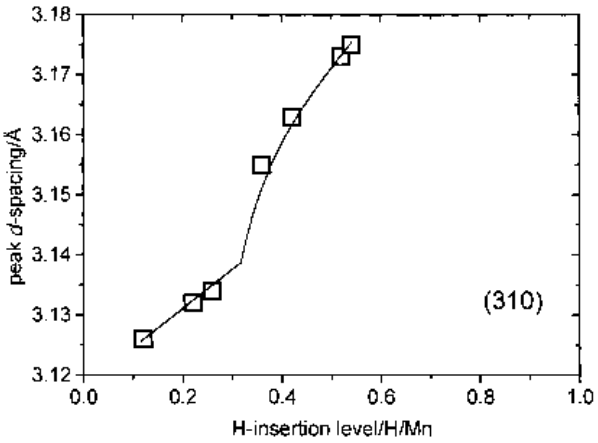

Fig. 6. Evolution of the peak *d* spacing against the H-insertion level for peak (3 1 0).

4. Discussion

4.1. *Location of inserted-H and maximum degree of H-insertion in the α-MnO_2 structure*

α-MnO_2 has 2,2-tunnels in its structure (Fig. 10). On each *a*,*b* plane, the tunnel can lodge a big cation, in

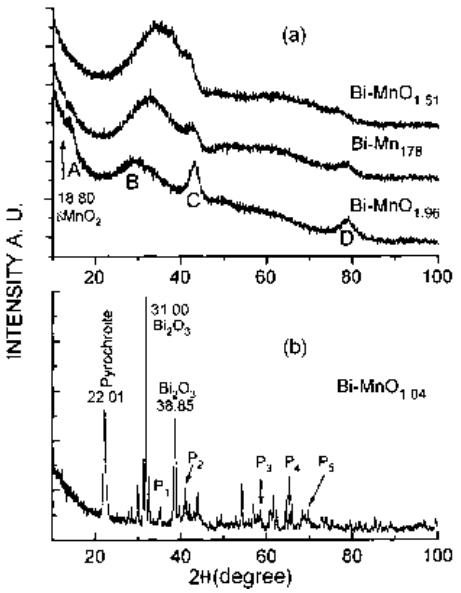

Fig. 8. XRD patterns of Bi-doped δ-MnO_2 samples: (a) for $x > 1.50$; (b) for $x = 1.04$. P_1, P_2, P_3 and P_4, are attributed to pyrochroite.

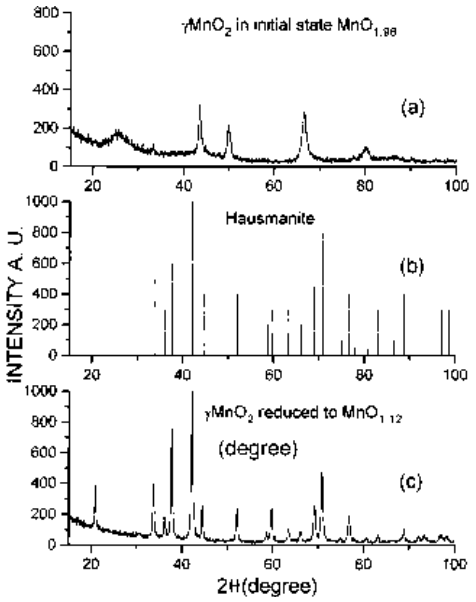

Fig. 9. XRD patterns of (a) γ-MnO_2 (Tekkosha) samples in the initial oxidation state ($MnO_{1.98}$); (b) hausmanite; (c) γ-MnO_2 (Tekkosha) in the most reduced state ($MnO_{1.12}$).

this case NH_4^+ ion, which stabilizes the lattice. Each tunnel is built with 8 Mn-atoms, but each Mn is associated with two tunnels. Thus, the ratio tunnel/Mn is 0.25. Each NH_4^+ being associated with one tunnel, the number n_{free} of NH_4^+-free tunnels is

$$n_{\text{free}} = 0.25 - n_{NH_4^+} \tag{5}$$

$n_{NH_4^+}$ is the number of tunnels occupied by the ion NH_4^+ (see Fig. 10).

By analogy with γ-MnO_2, protons are inserted in the tunnels. Thus, we can define the average H-occupation density of the tunnel (expressed as H/tunnel) by the ratio $R_{y/n_{\text{free}}}$:

$$\boldsymbol{R}_{y/n_{\text{free}}} = y/n_{\text{free}} \tag{6}$$

where y is defined by Relationship 3.

The size of 2,2-tunnels is about two times that of the 2,1 tunnels of γ-MnO_2. Thus, four protons should occupy the 2,2 tunnels. As the structure of hollandite remains stable for the average degree of oxidation down to $x \simeq 1.63$, the maximum degree of H-insertion (MHID) should be

$$H_{\text{ins.max}} = (1.94 - 1.63) \times 2 = \sim 0.62 \text{ H/Mn} \tag{7}$$

Figure 11 shows the variation of the ratio y/n_{free} against the average degree of oxidation. The ratio is close to 4 for samples α-$MnO_{1.68}$ to α-$MnO_{1.63}$ whereas the NH_4^+ content decreases (see Fig. 1). This result indicates a departure of the NH_4^+ ion and the resulting NH_4^+-free tunnel is occupied by 4 H-atoms.

For values of x less than ~ 1.63, the ratio increases above 4 and at the same time, a change of the structure occurs. Therefore, it appears that the forced-insertion of a supplementary H-atom into a tunnel occupied by one NH_4^+ ion or by four H-atoms causes the destruction of the lattice.

A similar calculation can be done for the reduction achieved by Gehain *et al.* [25] on a cryptomelane of formula $(K_{0.65}\ Ba_{0.02}\ Na_{0.08})Mn_8O_{16}$. According to this formula, there are 0.65 + 0.02 + 0.08 = 0.75 cations for 8 atoms of manganese. This corresponds to 3 cations per 8 channels, which implies 0.938 tunnels/Mn are occupied by the cations. The remaining cation-free tunnels correspond to 0.156 tunnels/Mn. If they are occupied by 4 H, the maximum degree of H-insertion should be 0.625 H/Mn. This value is very near the maximum degree of H-insertion for which the spinel structure is appearing. Practically, it is the same as the value found for α-MnO_2 stabilized by NH_4^+.

Discharge capacity measurements reported from the discharge tests carried out at $0.025\,\text{A g}^{-1}$ in 1 M KOH solution correspond to an insertion of ~0.63 H/Mn. Furthermore, in nonaqueous solvents, the discharge capacity corresponds to an insertion of ~0.65 Li/Mn [38]. Similar values between the maximum degrees of chemical H-insertion, electrochemical H-insertion in alkaline media and electrochemical Li-insertion in nonaqueous media, show that the charge-compensating ions mainly lodge in the free 2,2 tunnels whatever the insertion method used.

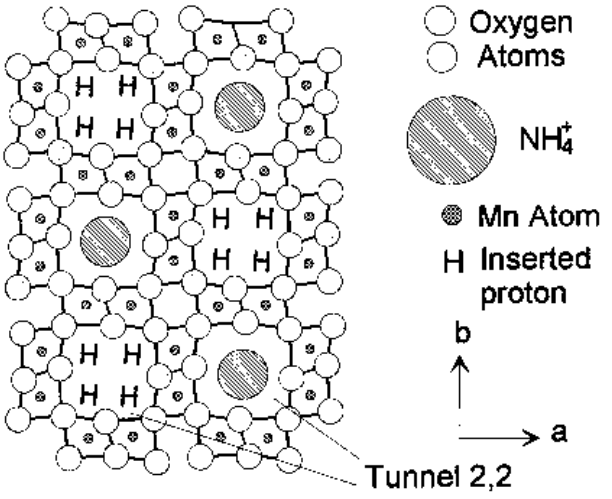

Fig. 10. Structure in the a, b plane of α-MnO_2 saturated with H.

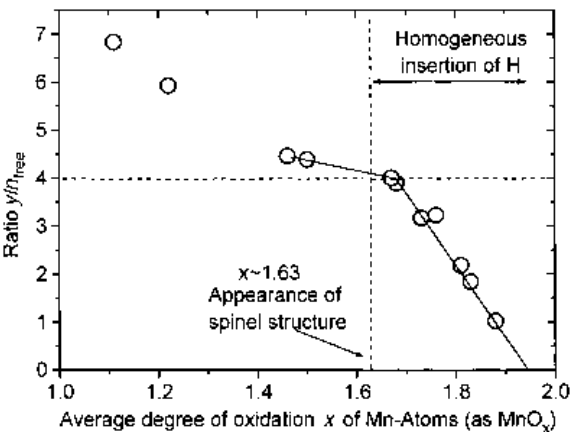

Fig. 11. Variation of the average H-occupation density of the tunnel expressed by the ratio y/n_{free} against the average degree of oxidation x.

The corresponding stabilizing-ion content is ~0.094 moles/Mn. This corresponds to the minimum content for which the hollandite structure remains stable.

4.2. *Formation of spinel structure and its consequence on the discharge capacity*

The spinel structure is not formed when the reduction is carried out with cinnamic alcohol in organic solvents, but only with hydrazine in aqueous solutions whatever the type of manganese dioxide. This result shows that the formation of a spinel structure does not take place in the solid phase, but likely through similar processes to those that occur in KOH media. The physical processes such as dissolution of MnOOH and $Mn(OH)_2$ (as $Mn(OH)_6^{3-}$ and $Mn(OH)_6^{2-}$, respectively) and the chemical processes (disproportionation or dehydration of $Mn(OH)_6^{3-}$) exist in both H_2N–NH_2 and KOH aqueous solutions. However, the kinetics of these physical and chemical processes would be different in these two media [11, 39].

From these data, the overall process leading to the spinel structure may be described as

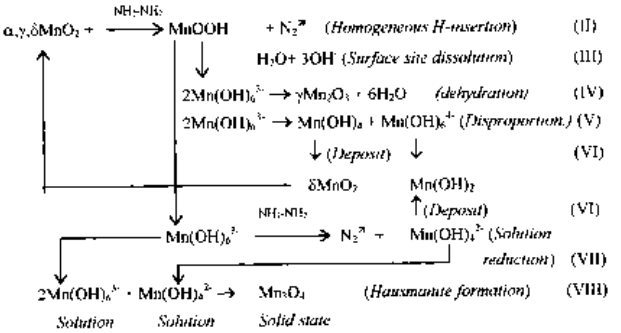

At first glance, it is possible to obtain γ-Mn_2O_3 and hausmanite as end-products through the Reactions IV and VIII, respectively. However, the formation of γ-Mn_2O_3 involves dehydration of the dissolved and hydrated species $Mn(OH)_3^{6-}$ in aqueous media. In the first place, this is not, *a priori*, a favourable condition for dehydration. In the second place, Reaction IV is competing with Reactions V, VII and VIII. The two first reactions lead to the formation of Mn(II), and thereby favour the formation of Mn_3O_4. Furthermore, when Zn^{2+} ions are present, published data show that the formation of hetaerolite $ZnMn_2O_4$ takes place [39–45] according to an overall reaction:

$$\underset{\text{Dissolved species}}{2\,Mn(III)} + ZnO_2H^- \rightarrow \underset{\text{Solid state}}{ZnMn_2O_4} + OH^- \quad \text{(IX)}$$

The dissolved Mn(III) species is identifiable with $Mn(OH)_3^{6-}$. Reaction IX is similar to Reaction VIII, and suggests that the building of hetaerolite and hausmanite lattices would involve similar processes.

Although they do not constitute a direct proof, all these data suggest that the spinel structure would be more stable when other ions such as Mn^{2+} or Zn^{2+} are present. Therefore, γ-Mn_2O_3 could exist if these two ions are absent. In reality, Reaction V provides Mn(II) species and in the more reduced state ($x < 1.33$), the dissolved Mn(II) species are always present. Thus, the formation of hausmanite could be more probable than that of γ-Mn_2O_3.

Reaction VIII can be seen as a complex-formation reaction between Mn(II) and Mn(III) species in which the resulting compound Mn_3O_4 could be a very stable complex, but having no significant electroactivity. Thereby, it is a dead-end reaction. If Bi(III) ions are present, Reaction VIII does not occur. Thus, the MnO_2 could be reversibly discharged with discharges greater than 1 F/Mn, and its cycle life would not be limited.

5. Conclusion

Various forms of MnO_2, progressively reduced by chemical methods, show the following lattice changes:

(i) With NH_4^+-α-MnO_2, the maximum degree of H-insertion (MHID) is ~0.62 H/Mn. Thus each NH_4^+-free tunnel is filled by four protons. This MHID is consistent with the discharge capacity during electrochemical reduction in a 1 M KOH solution (~0.65 F/Mn) and in non-aqueous media (~0.63 F/M). Such similar values show that Li^+ and H^+ ions occupy the same sites. The lowest degrees of oxidation are obtained when AHS are used. When the degree of H-insertion exceeds ~0.62 H/Mn, the lattice starts to disintegrate and cryptomelane progressively disappears while the spinel structure appears. A low degree of oxidation ($x < 1.33$) involves the existence of pyrochroite, but it is never observed in the XRD patterns. This is likely due to a poorly crystallized form of the pyrochroite.

(ii) With Bi-doped δ-MnO_2, the spinel structure is never observed even for H-insertion levels exceeding 1 H/Mn: the XRD pattern is dominated by the peaks of bismite (α-Bi_2O_3). This result shows the Bi-atoms hinder the formation of the spinel structure, but the XRD patterns do not allow us to establish the mechanism responsible for the absence of this structure.

(iii) When γ-MnO_2 (Tekkosha) is reduced to $MnO_{1.12}$, the XRD pattern only shows the spinel structure. Again, the peaks of pyrochroite are never observed. This is due to its ill-crystallized form. Finally such a poor crystallization of the pyrochroite appears to be characteristic of the reduction of MnO_2 samples by hydrazine in aqueous solutions.

Acknowledgement

This work is supported by Programme ECOTECH, appel 'Nouvelles Batteries'.

References

[1] K. Kordesch, M. Weissenbacher, *J. Power Sources* **51** (1994) 61.
[2] K. Kordesch, *U S Patent 4 105* 830 (1978).
[3] R. Chemelli, J. Gsellmann, G. Korbler and K. Kordesch, 'Manganese Dioxide Symposium', Vol.2, Tokyo (edited

and compiled by B. Schumm, Jr, H. M Joseph, and A. Kozawa), published by the I.C. MNO_2 Sample Office. PO Box, 6116, Cleveland, Ohio 44101, USA (1980) p. 150.
[4] K. Kordesch, J. Gsellmann, M. Peri, K. Tomantschger and R. Chemelli, *Electrochim. Acta* **26** (1981) 1495.
[5] W. Harer and K. Kordesch, 'The 2nd Battery Material Symposium', Vol.2, Graz, Austria (compiled by K. V. Kordesch and A. Kozawa), published by the International Battery Material Association (1985) p. 231.
[6] K. Kordesch, L. Binder W. Taucher, C. Faistauer and J. Daniel-Ivad, 'Symposium Power Sources 14, Research and Development in Non-Mechanical Electrical Power Sources' (The 18th International Power Sources) Stratford-upon-Avon, Apr. (1993) p. 193.
[7] Y. F. Yao, N. Gupta and H. S. Wroblowa, *J. Electroanal. Chem.* **223** (1987) 107.
[8] H. S. Wroblowa and N. Gupta, *ibid.* **238** (1987) 93.
[9] D. Y. Qu, B. E. Conway, L. Bai, Y. H. Zhou and W. A. Adams, *J. Appl. Electrochem.* **23** (1993) 693.
[10] H. Ouboumour, C. Cachet, M. Bodé, C. Lévy-Clément, J. Ginoux and L. T. Yu *Prog. Batteries & Battery Mater.* **12** (1994) 170.
[11] C. C. Castledine and B. E. Conway, *J Appl. Electrochem.* **24** (1995) 707.
[12] H. Ouboumour, C. Cachet, M. Bodé and L. T. Yu. *J. Electrochem. Soc.* **142** (1995) 1061.
[13] J. M. Tarascon and D. Guyomard, *Electrochim. Acta* **38** (1993) 1221.
[14] D. Guyomard and J. Tarascon, *J. Electrochem. Soc.* **140** (1993) 3071.
[15] J. P. Brenet, *Electrochim. Acta* **1** (1959) 231.
[16] W. C. Vosburgh, *J. Electrochem. Soc.* **106** (1959) 839.
[17] G. S. Bell and R. Huber, *ibid.* **111** (1964) 509.
[18] J. P. Gabano, B. Morignat, E. Fialdes, B. Emery and J.F. Laurent, *Z. Physik. Chim.* **46** (1965) 359.
[19] H. Bode and A. Schmier, *Chemie Ing. Techn.* **38** (1966) 651.
[20] D. Boden, C. J. Venuto, D. Wisler and R.B. Wylie, *J. Electrochem. Soc.* **115** (1968) 333
[21] J. Ambrose and G.W.D. Briggs, *J. Electroanal. Chem.* **21** (1971) 414.
[22] J. McBreen, *Power Sources* **5** (1975) 525.
[23] J. Fitzpatrick and F. L. Tye, *J. Appl. Electrochem.* **21** (1991) 130.
[24] C. Mondoloni, M. Laborde, J. Rioux, E. Andoni, and C. Levy-Clément, *J. Electrochem. Soc.* **139** (1992) 954.
[25] S. B. Kanungo, K. M. Desai and V. K. Dalal, *Electrochim. Acta* **26** (1981) 1147.
[26] J. B. Fernandes, B. D. Desai and V. K. Dalal, *Electrochim. Acta* **29** (1984) 181.
[27] E. D. Gehain, P. C. Picquet, C. J. Spears and F. L. Tye, *Prog. Battries & Battery Mater.* **13** (1994) 62.
[28] S. Donne, R. Fredlein, G. Lawrance, D. A. J. Swinkels and F. L. Tye, *ibid.* **13** (1994) 113.
[29] J. Bauer, O. H. Buss and O. G. Glemser, *Ber. Bunsenges Phys. Chem.* **89** (1985) 1070.
[30] J. Bauer, O. H. Buss and O. G. Glemser, *ibid.* **90** (1986) 809.
[31] J. Brenet, *Bull. Soc. Chim.* (1987) 9.
[32] F. Fillaux, H. Ouboumour, J. Tomkinson and L. T. Yu. *Chem. Phys.* **149** (1991) 459.
[33] P. Ruetschi, *J. Electrochem. Soc.* **131** (1984) 2737.
[34] M. Bodé, Thèse de Doctorat, Université Paris Val de Marne (1993).
[35] K. M. Parida, S. B. Kanungo and B. R. Sant, *Electrochim. Acta* **26** (1981) 435.
[36] F. Lubin, Thèse de Doctorat, Université de Rennes (1991).
[37] D. G Malpas and F. L. Tye, 'Handbook of Manganese Dioxide Battery Grade,' (edited by D. Glover, B. Schumm and A. Kozawa), International Battery Material Association, Brunswick OH, USA (1989) p. 177.
[38] P. Botkovitz, 'Thése de Dectorat', Institut des Matériaux, Université de Nantes (1993).
[39] A. Kozawa and J. F. Yeager, *J. Electrochem. Soc.* **112** (1965) 959.
[40] L. C. Copeland and F. S. Griffith, *Trans. Electrochem. Soc.* **89** (1946) 495.
[41] H. P. McMurdie, D. N. Craig and G. W. Vinal, *Trans. Electrochem. Soc.* **90** (1946) 509.
[42] K. Miyazaki, *J. Electroanal. Chem.* **21** (1969) 414.
[43] *Idem*, *J. Electrochem. Soc.*, **116** (1969) 1469.
[44] *Idem*, *ibid.* **117** (1970) 821.
[45] J. McBreen, 'Manganese Dioxide Symposium', Vol. 1, Cleveland (compiled by A. Kozawa and R. J. Brodd for the I.C. Sample Office of the Cleveland Section of the The Electrochemical Society), published by the I.C. Sample Office c/o Union Carbide Corporation, Parma Technical Center, PO Box, 6116, Cleveland, OH 44101, USA (1975) p. 97.